Supporting Information for **N-Rich Porous Carbons with Tunable Affinity for CO_2 Adsorption Achieve Size-Sieving Selectivity in Turbostratic Interlayers**

*James N. Burrow, J. Ehren Eichler, Yu Wang, David C. Calabro, and C. Buddie Mullins**

J. N. Burrow, Prof. C. B. Mullins
John J. McKetta Department of Chemical Engineering, The University of Texas at Austin, Austin, Texas 78712, United States
E-mail: mullins@che.utexas.edu

J. E. Eichler, Prof. C. B. Mullins
Department of Chemistry, The University of Texas at Austin, Austin, Texas 78712, United States

Dr. Y. Wang, Dr. D. C. Calabro
Corporate Strategic Research, ExxonMobil Research and Engineering Company, Annandale, New Jersey 08801, United States

Prof. C. B. Mullins
Texas Materials Institute, The University of Texas at Austin, Austin, Texas 78712, United States

Summary: additional characterization and analysis details related to material properties, isotherm models, selectivity, and process performance

Table of Contents

The Python scripts required for batch processing of IAST selectivity and TSA estimation can be found on Github here:

https://github.com/jeeichler/AdsorptionAnalysis

Table S1. Summary of physicochemical properties of the SMx carbons.

	BET (m^2/g)	V_{pore} <1nm (cc/g)	V_{pore} <2nm (cc/g)	V_{pore} <200nm (cc/g)	C 1s (at%)	N 1s (at%)	O 1s (at%)	XPS N/C	CHN EA N/C	*002* Peak (°)	d_{002} (Å)	FWHM (°)	L_c (Å)
SM0-PYRO	0.8	--	--	--	96.0	0.0	4.0	0	0	22.40	3.97	10.81	7.41
SM20-PYRO	4.9	--	--	--	81.0	16.9	2.2	0.20	0.21	25.04	3.56	9.50	8.48
SM40-PYRO	1.3	--	--	--	77.4	19.0	3.6	0.25	0.29	25.39	3.51	9.32	8.65
SM60-PYRO	2.9	--	--	--	76.0	20.3	3.7	0.27	0.35	25.68	3.47	7.65	10.5
SM80-PYRO	40	--	--	--	75.1	21.5	3.4	0.29	0.34	25.45	3.50	7.79	10.4
SM0-OX-0.5	857	0.29	0.30	0.38	81.8	0.0	18.2	0	0	20.21	4.39	17.59	4.54
SM10-OX-0.5	1570	0.41	0.52	0.62	86.5	7.2	6.4	0.08	0.08	22.86	3.89	17.41	4.61
SM20-OX-0.5	1210	0.27	0.38	0.54	82.6	12.0	5.4	0.15	0.17	24.56	3.62	11.08	7.26
SM30-OX-0.5	1130	0.27	0.35	0.52	81.4	13.7	4.9	0.17	0.18	25.01	3.56	9.69	8.31
SM40-OX-0.5	816	0.20	0.26	0.34	79.0	16.8	4.2	0.21	0.23	25.39	3.51	8.27	9.75
SM50-OX-0.5	842	0.22	0.28	0.34	78.3	16.0	5.7	0.20	0.24	25.64	3.47	7.31	11.0
SM60-OX-0.5	725	0.17	0.23	0.32	75.4	18.8	5.8	0.25	0.36	26.46	3.37	4.11	19.7
SM70-OX-0.5	601	0.16	0.20	0.28	74.7	19.3	6.0	0.26	0.38	26.78	3.33	3.34	24.2
SM80-OX-0.5	528	0.15	0.18	0.27	73.7	22.1	4.2	0.30	0.41	26.85	3.32	3.00	26.9
SM0-OX-1	943	0.32	0.33	0.42	84.0	0.0	16.0	0	0	19.84	4.47	21.64	3.69
SM10-OX-1	2500	0.48	0.72	1.06	89.1	1.6	9.3	0.02	0	19.19	4.62	23.39	3.41
SM20-OX-1	2740	0.37	0.69	1.33	88.3	5.7	6.0	0.06	0.07	20.48	4.34	20.56	3.89
SM30-OX-1	2660	0.35	0.64	1.39	87.4	9.0	3.6	0.10	0.12	22.58	3.94	20.23	3.96
SM40-OX-1	2040	0.31	0.56	1.06	84.7	12.0	3.4	0.14	0.16	23.88	3.73	14.11	5.70
SM50-OX-1	1580	0.24	0.37	0.87	86.2	9.9	3.8	0.12	0.18	23.42	3.80	13.06	6.15
SM60-OX-1	834	0.16	0.25	0.45	79.1	17.0	3.9	0.28	0.28	26.18	3.40	5.90	13.7
SM70-OX-1	754	0.13	0.22	0.47	78.2	15.9	5.9	0.20	0.36	26.75	3.33	3.23	25.0
SM80-OX-1	670	0.13	0.21	0.41	75.8	19.7	4.5	0.26	0.39	26.80	3.33	2.95	27.4

Table S2. Detailed surface chemistry of the SMx carbons as determined by XPS.

	C=C (at%)	C-N / C-C (at%)	CN_3 / COH (at%)	CO (at%)	C-N=C (at%)	C_2NH (at%)	NC_3 (at%)	NO_x (at%)	CO / NO (at%)	OH (at%)
SM0-PYRO	69.1	18.2	5.8	2.9	0.0	0.0	0.0	0.0	2.8	2.4
SM20-PYRO	29.9	38.9	9.3	2.9	6.5	2.8	4.8	2.8	2.4	1.2
SM40-PYRO	23.6	41.9	8.9	2.9	9.0	3.2	5.6	1.2	3.1	0.5
SM60-PYRO	25.8	39.2	8.5	2.5	9.7	3.5	5.8	1.3	3.0	0.8
SM80-PYRO	25.2	36.7	9.8	3.5	9.9	3.9	6.1	1.5	2.4	1.1
SM0-OX-0.5	59.9	15.4	0.0	6.5	0.0	0.0	0.0	0.0	4.8	14.3
SM10-OX-0.5	39.4	33.6	9.1	4.4	2.6	2.8	1.1	0.7	3.5	2.7
SM20-OX-0.5	33.0	36.5	9.1	4.0	5.1	3.8	2.1	1.0	2.4	3.0
SM30-OX-0.5	32.0	36.8	8.6	4.0	6.2	4.6	1.9	1.1	2.3	2.6
SM40-OX-0.5	29.8	40.6	6.7	2.0	8.3	5.4	2.1	1.0	1.4	2.8
SM50-OX-0.5	34.9	33.0	7.9	2.5	8.0	5.2	1.7	1.2	3.0	2.8
SM60-OX-0.5	27.8	39.6	6.0	2.0	9.6	6.1	1.8	1.3	2.1	3.6
SM70-OX-0.5	26.6	40.6	5.5	2.1	10.4	5.3	2.1	1.5	2.6	3.4
SM80-OX-0.5	24.4	41.6	5.6	2.2	12.2	6.4	2.3	1.2	1.4	2.8
SM0-OX-1	63.0	16.8	0.0	4.2	0.0	0.0	0.0	0.0	6.2	9.8
SM10-OX-1	46.0	30.5	9.2	3.4	0.2	0.7	0.4	0.3	5.7	3.6
SM20-OX-1	38.8	33.9	10.0	5.6	1.8	2.5	0.8	0.6	2.3	3.7
SM30-OX-1	34.9	35.9	10.3	6.3	3.4	3.0	1.4	1.2	1.5	1.8
SM40-OX-1	46.1	22.7	11.2	4.7	5.2	3.9	2.0	0.8	1.7	1.7
SM50-OX-1	34.4	38.7	8.9	4.2	4.1	3.1	1.5	1.1	2.1	1.7
SM60-OX-1	24.5	45.1	7.0	2.5	8.9	5.4	1.8	0.9	1.7	2.2
SM70-OX-1	26.2	41.8	7.4	2.8	8.4	4.9	2.0	0.6	2.8	3.1
SM80-OX-1	27.8	41.2	5.0	1.9	11.4	5.4	2.4	0.5	1.5	3.0

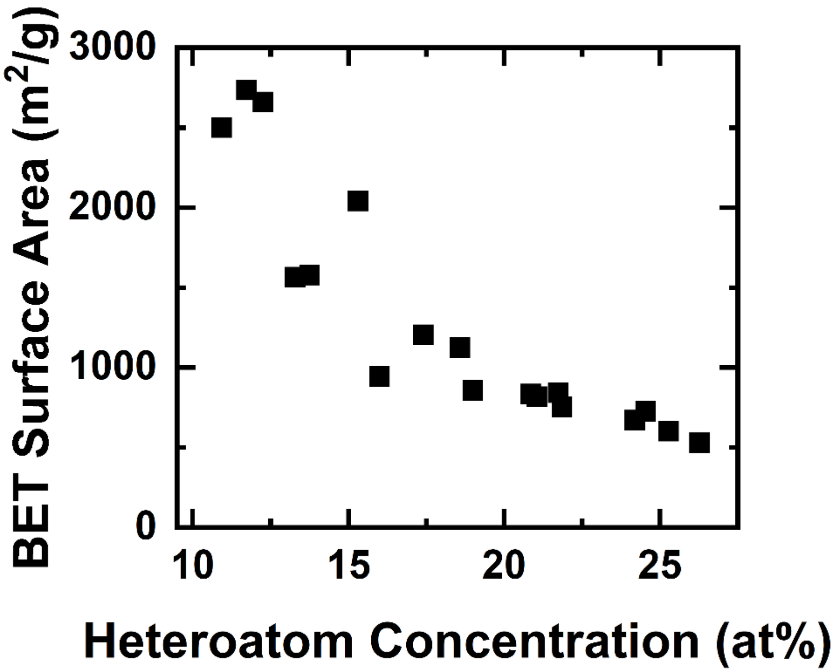

Figure S1. As heteroatom (N and O) content increased, surface area and porosity decreased.

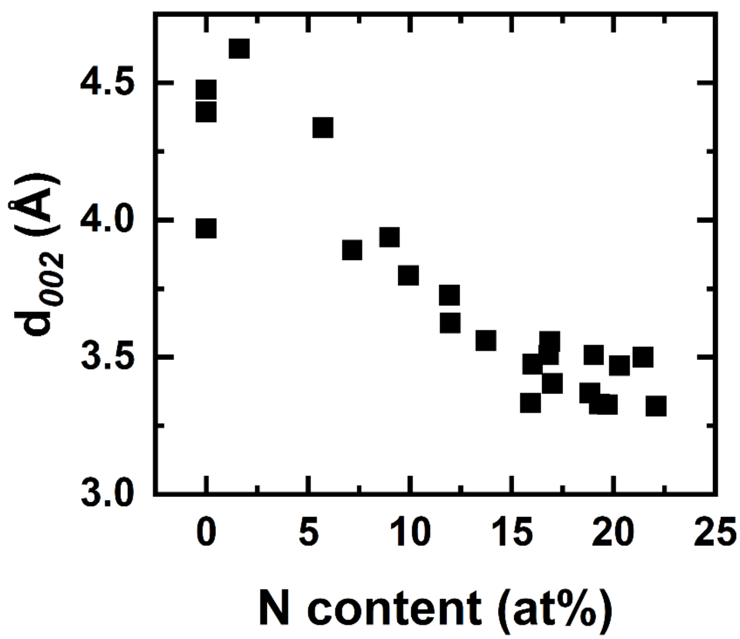

Figure S2. The average interlayer spacing of the turbostratic carbons was a strong function of N content.

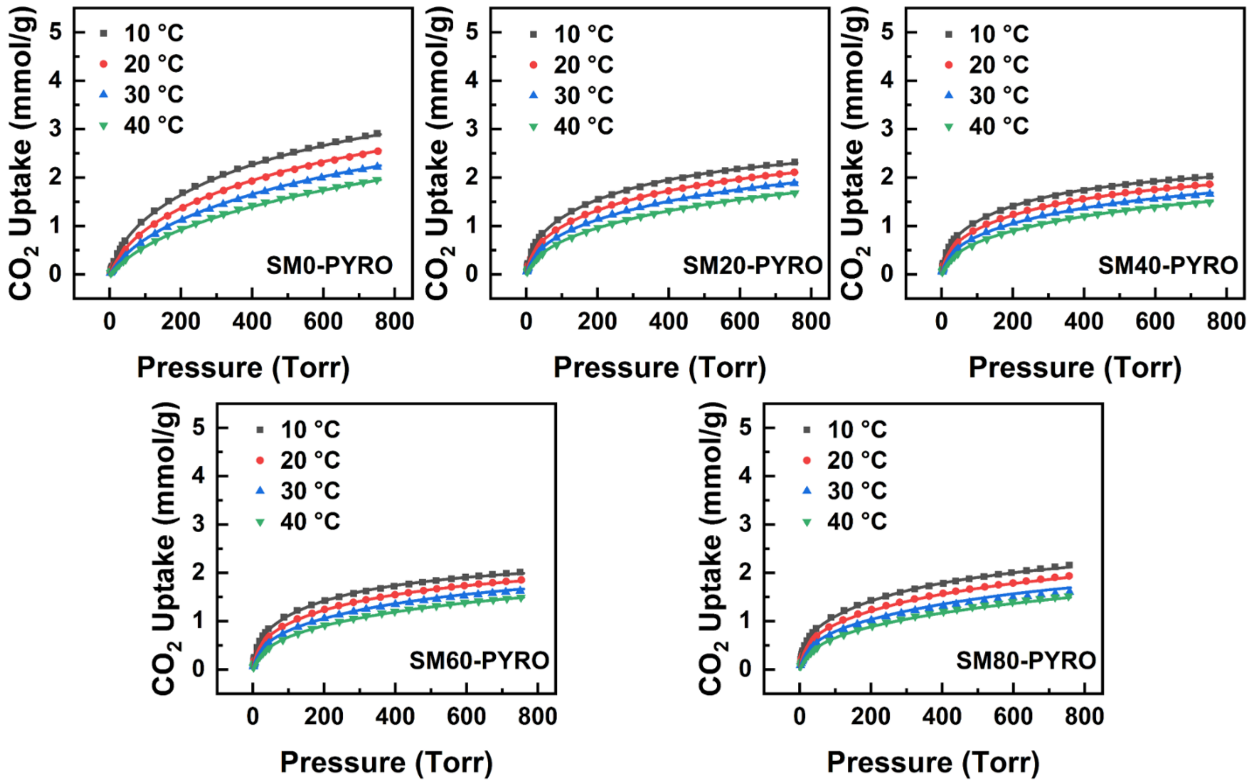

Figure S3. Variable temperature CO_2 isotherms of pyrolyzed samples, with raw data (symbols) and dual-site Langmuir fits (lines).

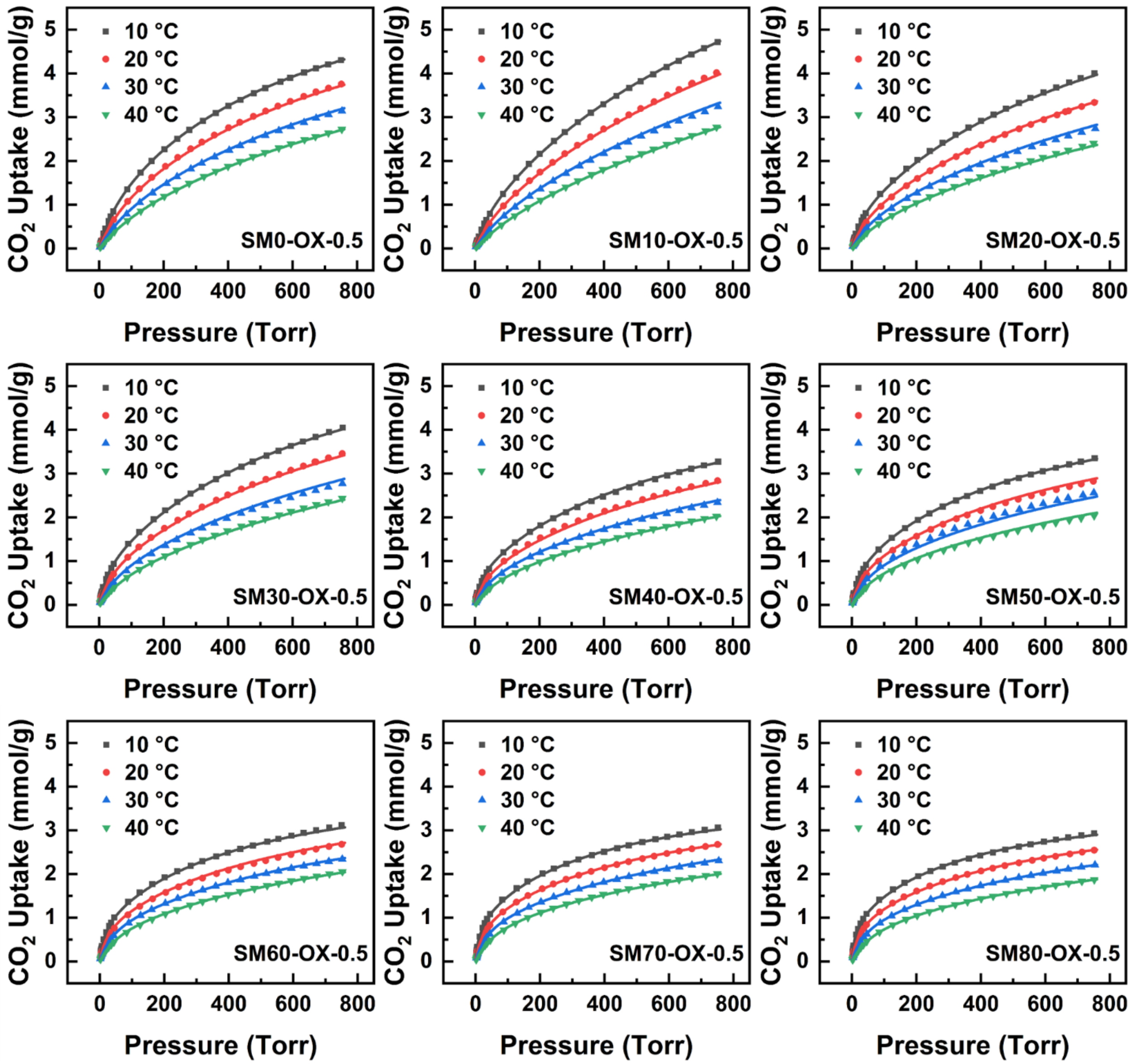

Figure S4. Variable temperature CO_2 isotherms of the OX-0.5 activated samples, with raw data (symbols) and dual-site Langmuir fits (lines).

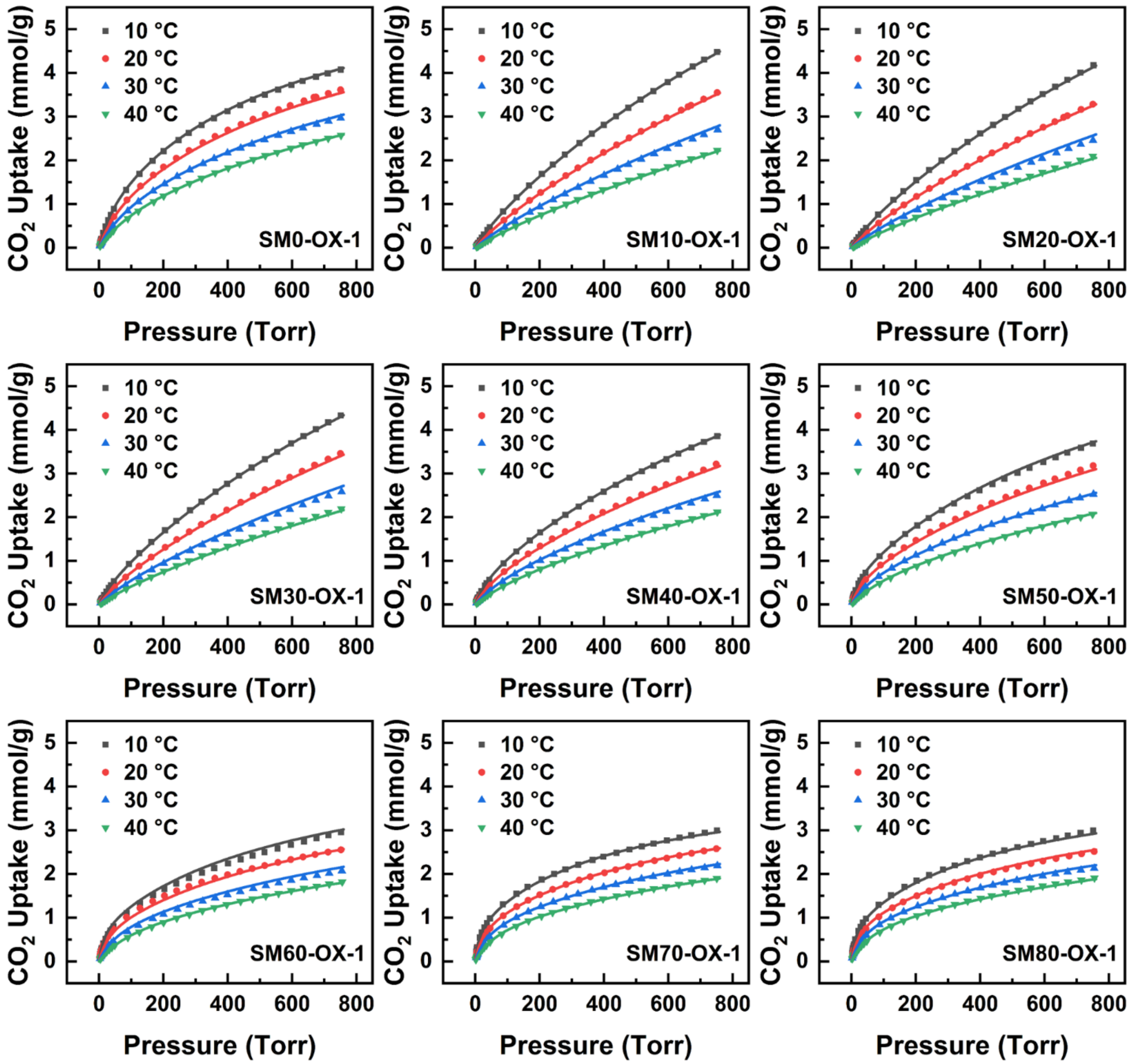

Figure S5. Variable temperature CO_2 isotherms of the OX-1 activated samples, with raw data (symbols) and dual-site Langmuir fits (lines).

Table S3. Temperature-dependent dual site Langmuir fits and statistics for CO_2 adsorption.

	$q_{A,sat}$ (mmol/g)	$q_{B,sat}$ (mmol/g)	ΔH_A (kJ/mol)	ΔS_A (J/mol K)	ΔH_B (kJ/mol)	ΔS_B (J/mol K)	Adj. R^2
SM0-PYRO	0.87 ±0.02	3.70 ±0.02	-29.00 ±1.53	-52.18 ±5.16	-20.41 ±0.79	-44.04 ±2.67	0.99997
SM20-PYRO	0.65 ±0.02	2.31 ±0.01	-36.71 ±0.47	-67.17 ±1.57	-23.53 ±0.14	-49.29 ±0.45	0.99980
SM40-PYRO	0.63 ±0.02	1.87 ±0.01	-35.01 ±0.54	-60.36 ±1.80	-24.83 ±0.55	-52.60 ±1.83	0.99971
SM60-PYRO	0.66 ±0.02	1.79 ±0.01	-36.62 ±0.24	-65.05 ±0.81	-25.92 ±1.23	-56.38 ±4.14	0.99964
SM80-PYRO	0.71 ±0.02	2.12 ±0.03	-37.70 ±0.35	-69.62 ±1.17	-26.14 ±3.43	-60.32 ±11.52	0.99937
SM0-OX-0.5	0.93 ±0.03	6.42 ±0.02	-28.67 ±0.75	-51.80 ±2.52	-21.28 ±0.77	-47.83 ±2.58	0.99999
SM10-OX-0.5	0.81 ±0.03	9.89 ±0.12	-33.18 ±0.96	-67.21 ±3.22	-19.57 ±1.03	-46.30 ±3.46	0.99997
SM20-OX-0.5	0.80 ±0.02	7.01 ±0.08	-34.15 ±1.50	-66.79 ±5.03	-21.61 ±1.43	-51.63 ±4.82	0.99993
SM30-OX-0.5	0.87 ±0.02	6.33 ±0.07	-37.56 ±0.67	-76.92 ±2.24	-23.46 ±1.63	-56.67 ±5.47	0.99991
SM40-OX-0.5	0.76 ±0.02	4.64 ±0.05	-36.32 ±2.24	-70.75 ±7.55	-23.76 ±1.16	-56.40 ±3.91	0.99985
SM50-OX-0.5	0.84 ±0.02	4.36 ±0.04	-35.09 ±2.89	-65.15 ±9.73	-25.43 ±2.60	-60.54 ±8.76	0.99988
SM60-OX-0.5	0.83 ±0.02	3.60 ±0.03	-39.36 ±1.34	-78.16 ±4.50	-25.21 ±1.07	-58.44 ±3.61	0.99976
SM70-OX-0.5	0.89 ±0.02	3.20 ±0.02	-40.61 ±0.56	-81.66 ±1.89	-28.30 ±0.56	-67.89 ±1.89	0.99976
SM80-OX-0.5	0.89 ±0.02	2.93 ±0.02	-46.99 ±1.23	-103.10 ±4.21	-30.85 ±0.24	-76.32 ±0.83	0.99975
SM0-OX-1	0.95 ±0.03	5.76 ±0.03	-24.52 ±1.49	-36.38 ±5.01	-23.11 ±1.39	-53.56 ±4.69	0.99996
SM10-OX-1	0.34 ±0.03	15.40 ±0.28	-25.25 ±2.40	-42.610 ±8.07	-20.62 ±0.90	-54.93 ±3.01	0.99998
SM20-OX-1	0.33 ±0.02	14.82 ±0.26	-29.95 ±2.49	-57.89 ±8.37	-20.50 ±1.42	-54.99 ±4.77	0.99998
SM30-OX-1	0.43 ±0.02	13.82 ±0.26	-32.03 ±1.17	-64.42 ±3.93	-21.14 ±1.51	-56.22 ±5.09	0.99997
SM40-OX-1	0.60 ±0.02	10.29 ±0.17	-34.09 ±2.13	-69.71 ±7.16	-20.26 ±1.18	-51.61 ±3.96	0.99997
SM50-OX-1	0.64 ±0.02	7.13 ±0.11	-41.79 ±2.16	-90.90 ±7.26	-22.92 ±1.29	-56.96 ±4.33	0.99989
SM60-OX-1	0.84 ±0.03	4.15 ±0.10	-42.44 ±9.19	-91.78 ±30.4	-26.51 ±3.85	-66.55 ±13.12	0.99951
SM70-OX-1	0.83 ±0.02	3.42 ±0.03	-39.27 ±0.19	-77.87 ±0.64	-27.50 ±0.64	-66.73 ±2.16	0.99975
SM80-OX-1	0.88 ±0.02	3.45 ±0.05	-38.16 ±1.54	-74.20 ±5.17	-26.89 ±1.92	-65.54 ±6.46	0.9996

Table S4. Henry's constants for CO_2 and N_2 at 30 °C and resulting Henry's selectivity.

	k_{CO_2} (mmol/g*bar)	k_{N_2} (mmol/g*bar)	$S_{Henry's}$ (-)
SM0-PYRO	8.91	0.399	22
SM20-PYRO	19.9	0.294	68
SM40-PYRO	21.5	0.185	117
SM60-PYRO	23.9	0.242	98
SM80-PYRO	22.4	0.199	113
SM0-OX-0.5	10.1	0.580	17
SM10-OX-0.5	8.73	0.581	15
SM20-OX-0.5	10.9	0.367	30
SM30-OX-0.5	13.0	0.358	36
SM40-OX-0.5	13.7	0.283	49
SM50-OX-0.5	17.7	0.247	72
SM60-OX-0.5	19.5	0.222	88
SM70-OX-0.5	22.0	0.178	124
SM80-OX-0.5	20.9	0.134	156
SM0-OX-1	11.5	0.508	23
SM10-OX-1	4.79	0.444	11
SM20-OX-1	4.53	0.332	14
SM30-OX-1	5.25	0.333	16
SM40-OX-1	6.62	0.286	23
SM50-OX-1	9.94	0.188	53
SM60-OX-1	13.1	0.182	72
SM70-OX-1	19.1	0.146	130
SM80-OX-1	19.9	0.171	116

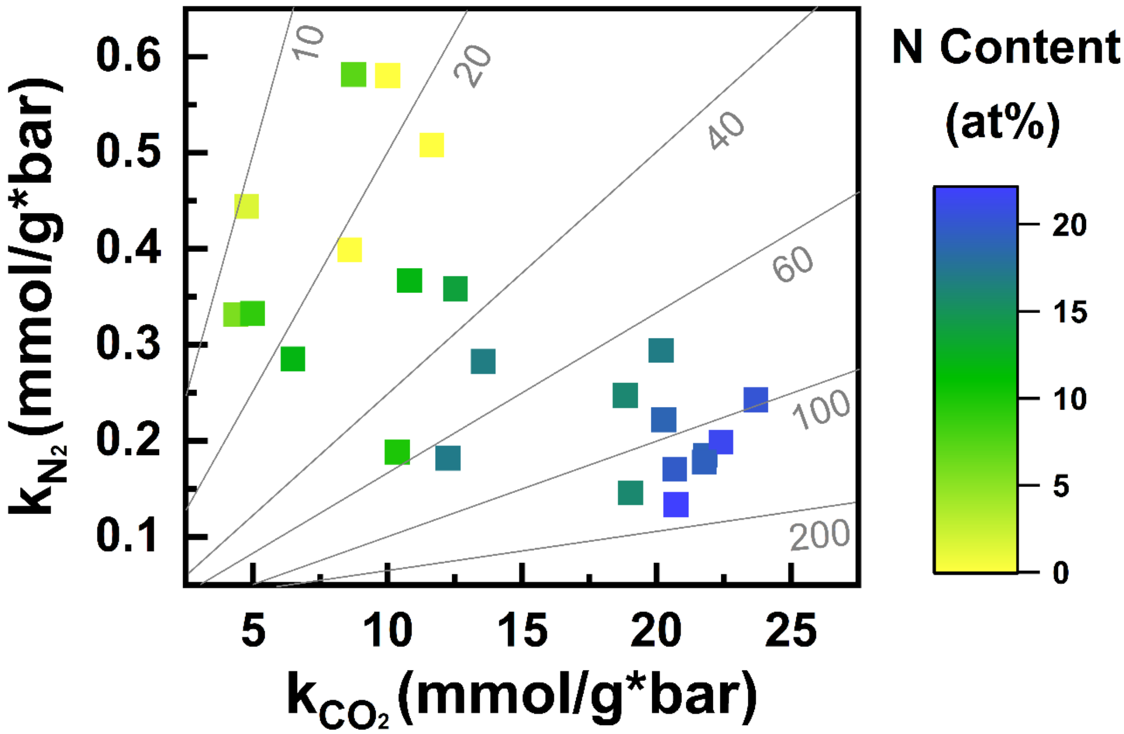

Figure S6. Comparison of Henry's constants for CO_2 and N_2. Grey lines indicate Henry's selectivity.

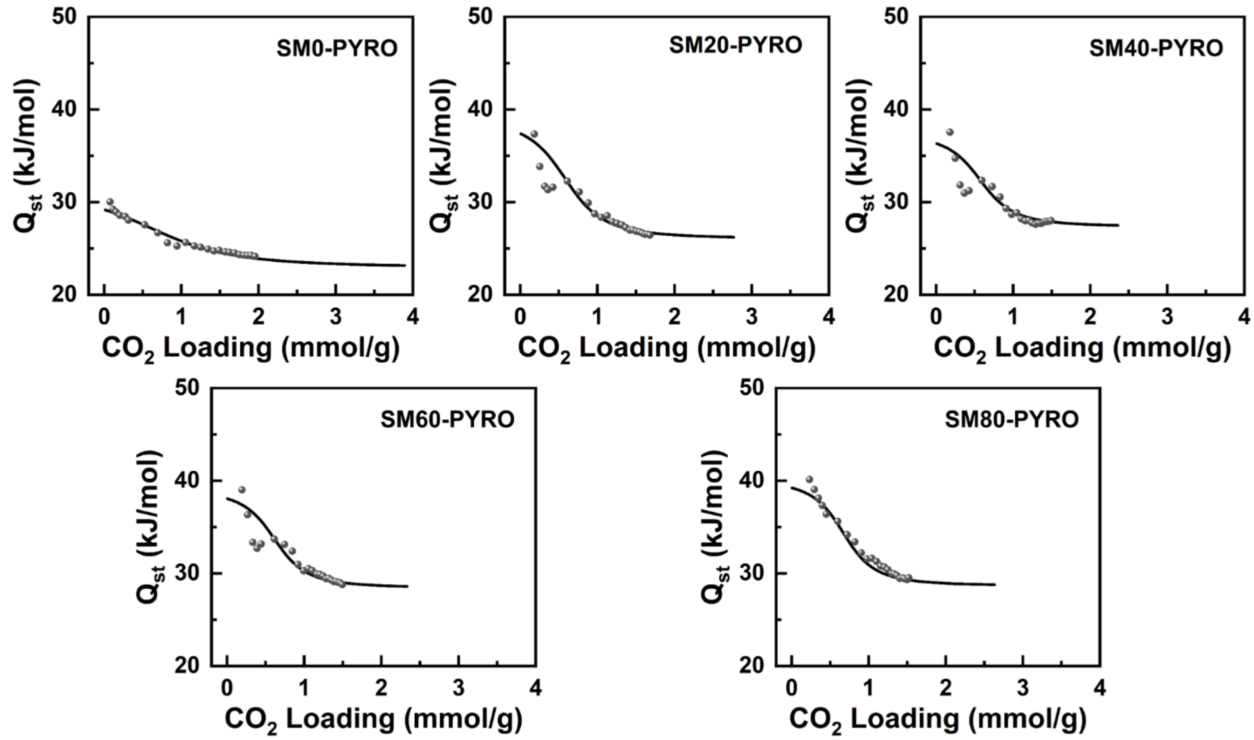

Figure S7. Comparison of analytical (lines) vs. numerically-derived (symbols) isosteric heats of adsorption for pyrolyzed samples.

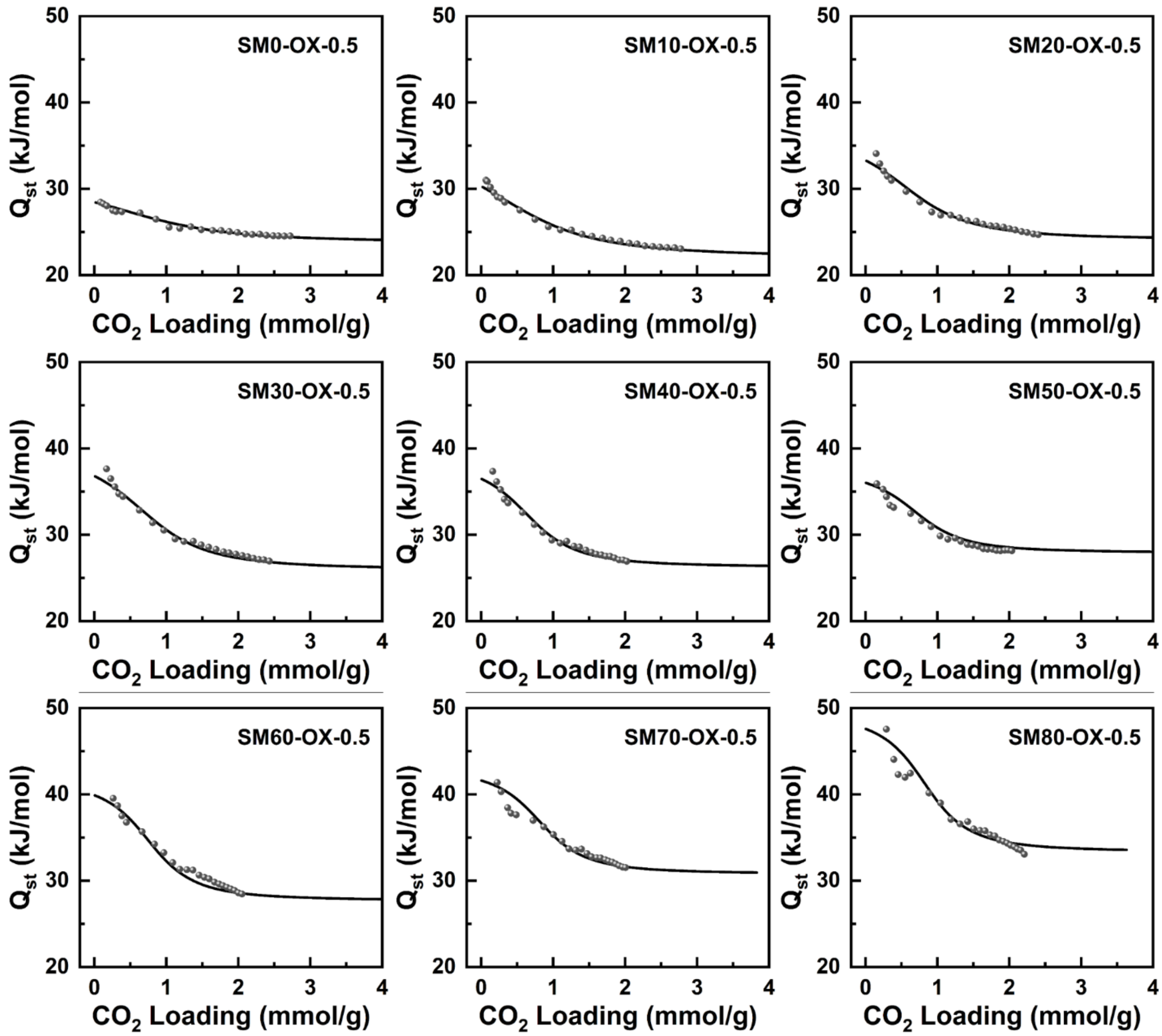

Figure S8. Comparison of analytical (lines) vs. numerically-derived (symbols) isosteric heats of adsorption for activated SMx-OX-0.5 samples.

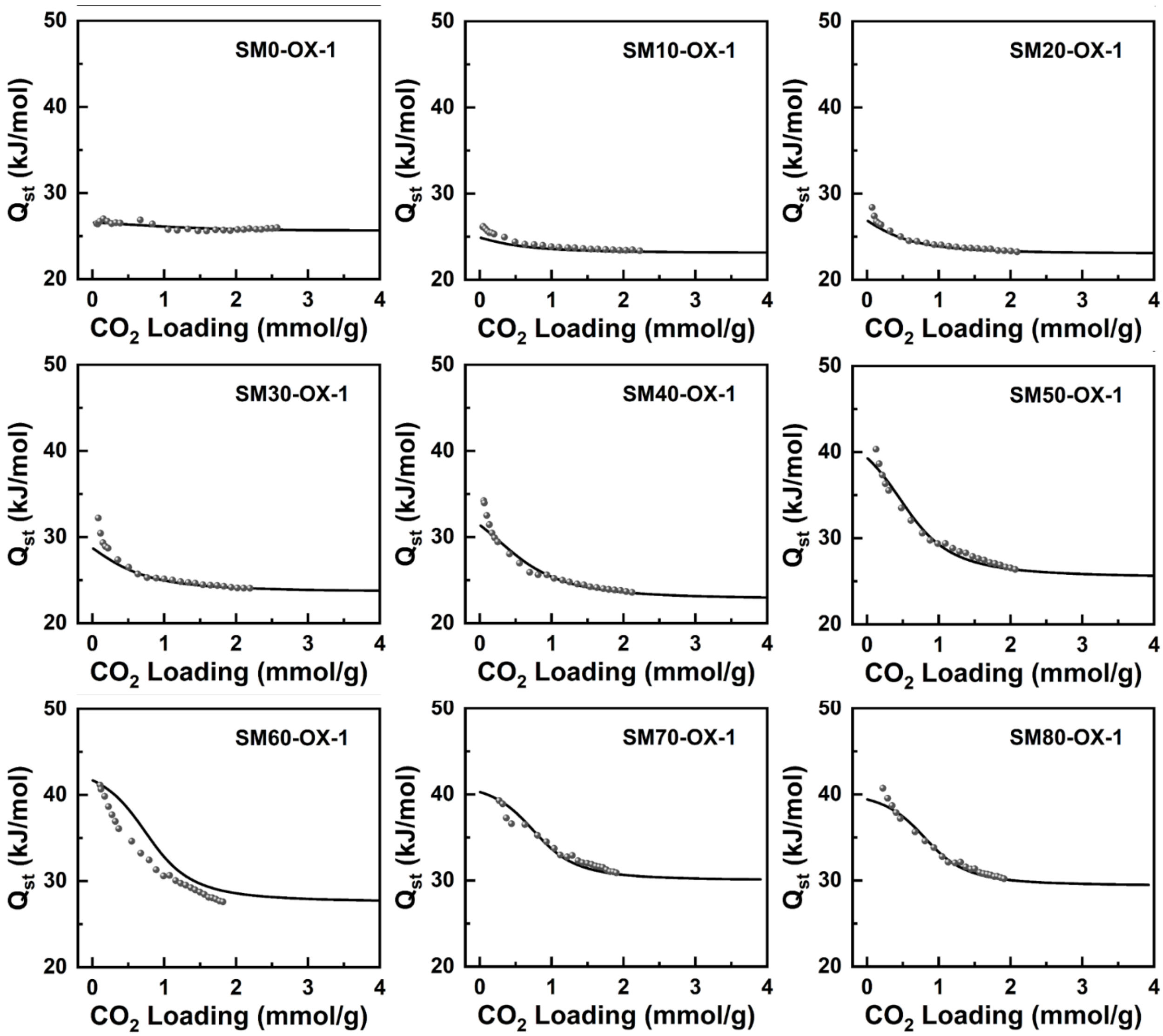

Figure S9. Comparison of analytical (lines) vs. numerically-derived (symbols) isosteric heats of adsorption for activated SMx-OX-1 samples.

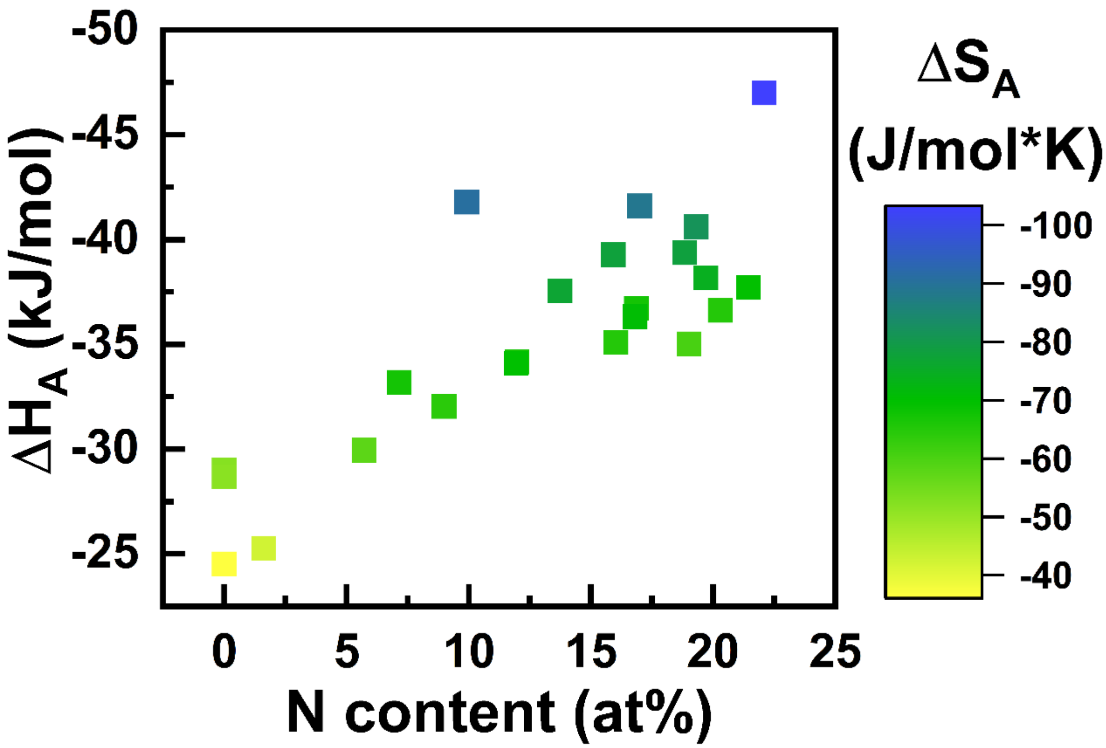

Figure S10. At a given N content, increases in the magnitude of entropy loss upon adsorption (most likely associated with confinement; heat map) resulted in increased enthalpy gained upon adsorption.

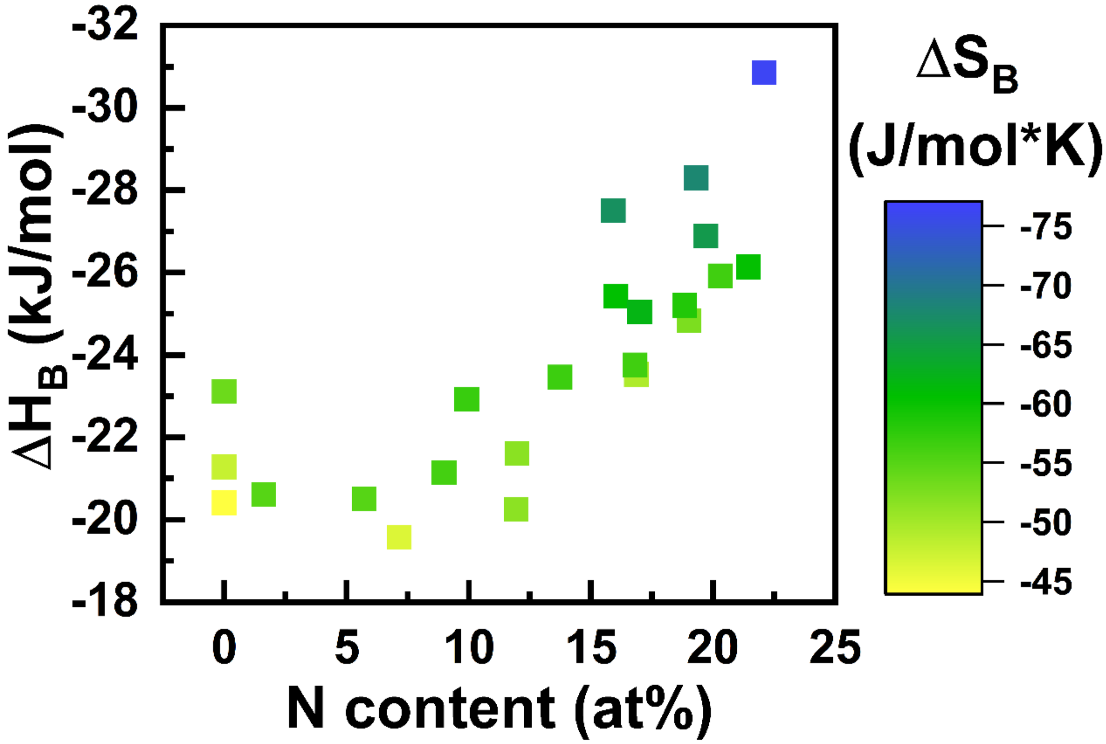

Figure S11. At a given N content, increases in the magnitude of entropy loss upon adsorption (most likely associated with confinement; heat map) resulted in increased enthalpy gained upon adsorption.

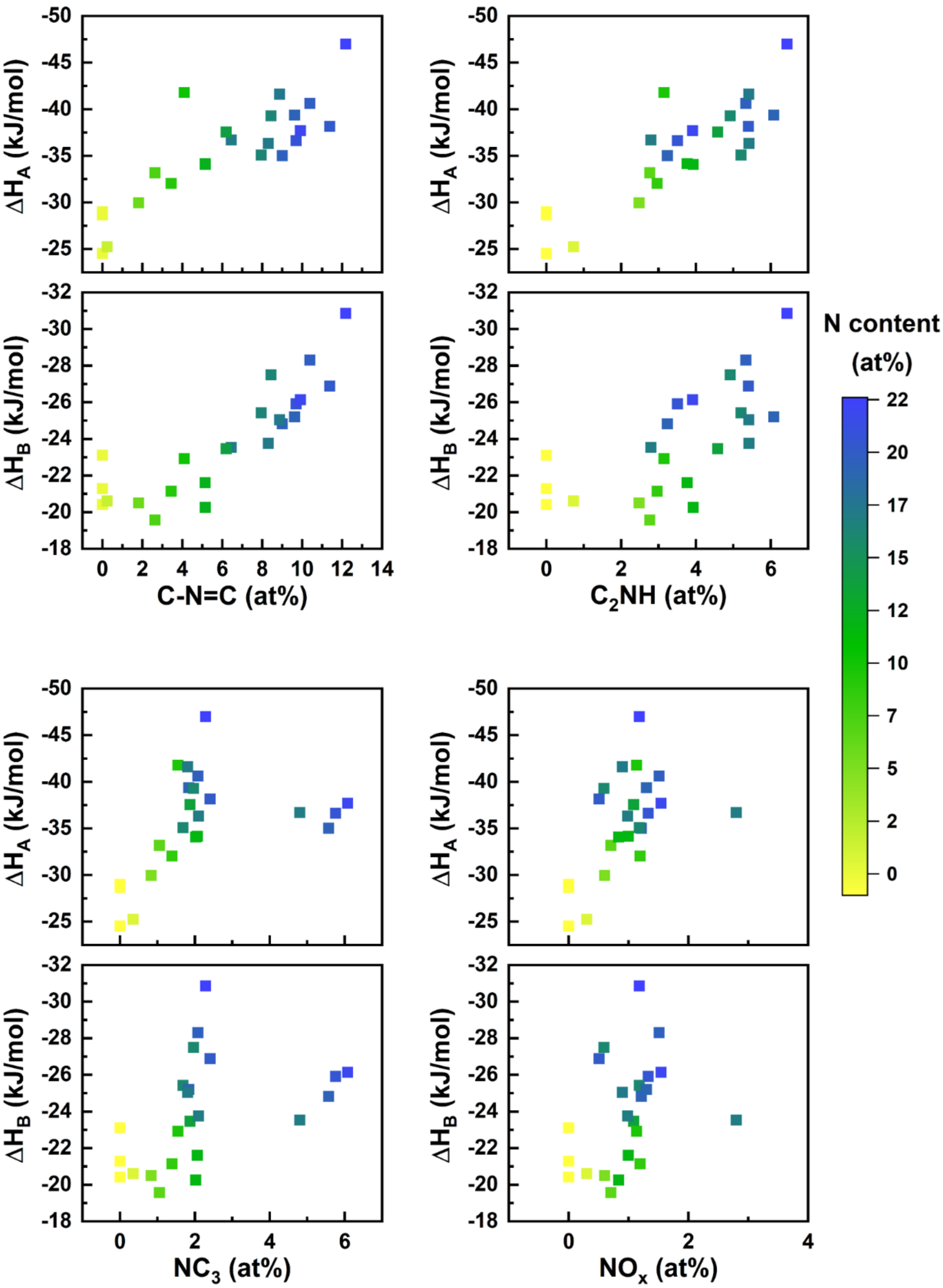

Figure S12. Correlations between different N functionalities present on the carbons' surfaces (as determined by XPS) and the observed enthalpies of adsorption for both the strong (A) and weak (B) site. Overall, it seems that pyridinic N (C-N=C, top left) has the largest relative effect on increasing the adsorptive affinity for CO_2, followed by pyrollic (C_2NH, top right), then graphitic (NC_3, bottom left), then oxidized N species (NO_x, bottom right).

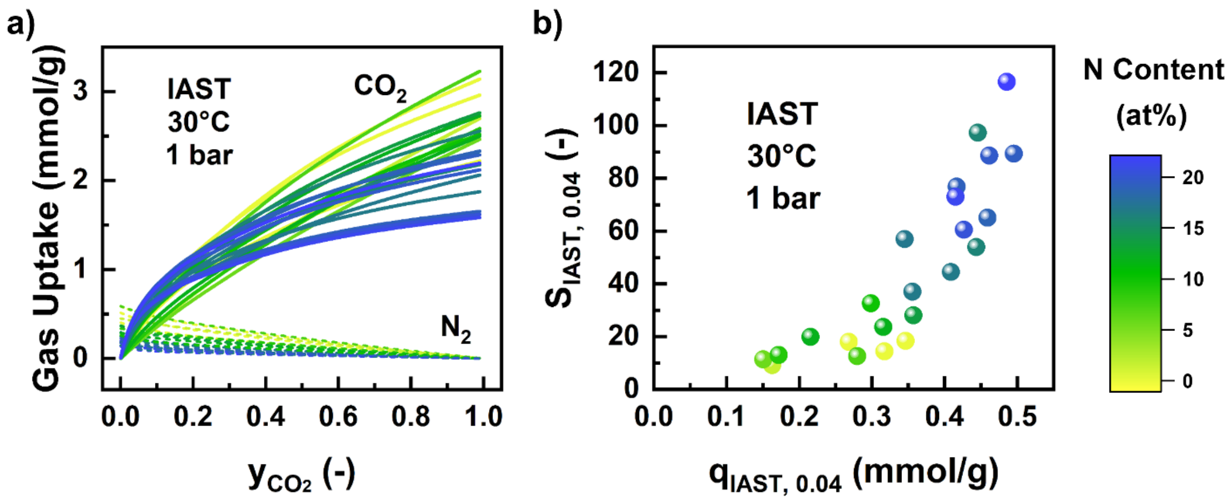

Figure S13. IAST predictions as quantified by a) binary isotherms and b) estimated CO_2 capacity and selectivity for a feed with 4% CO_2 at 30 °C and 1 bar of total pressure.

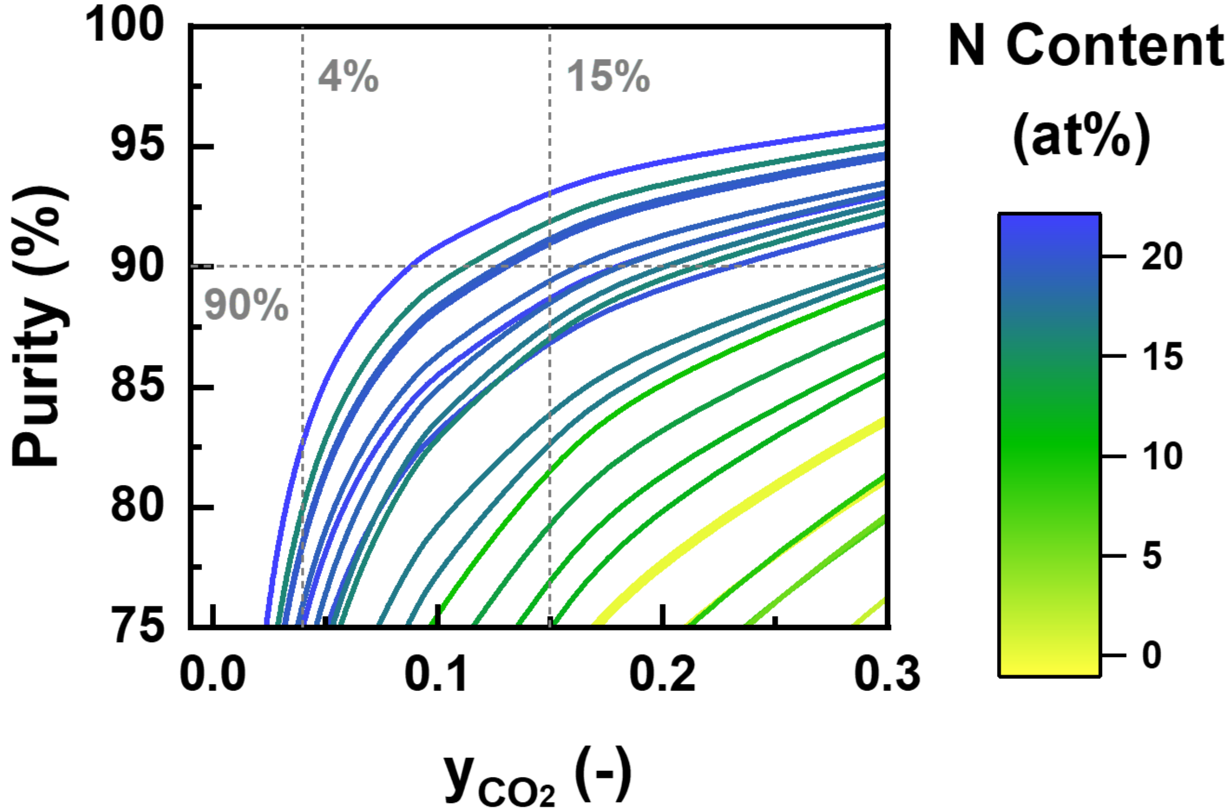

Figure S14. A zoomed-in purity plot focusing on the purity and concentration ranges of interest for practical implementation of carbon capture. Predictions by IAST at 30 °C for a binary feed of CO_2 and N_2 at 1 bar total pressure.

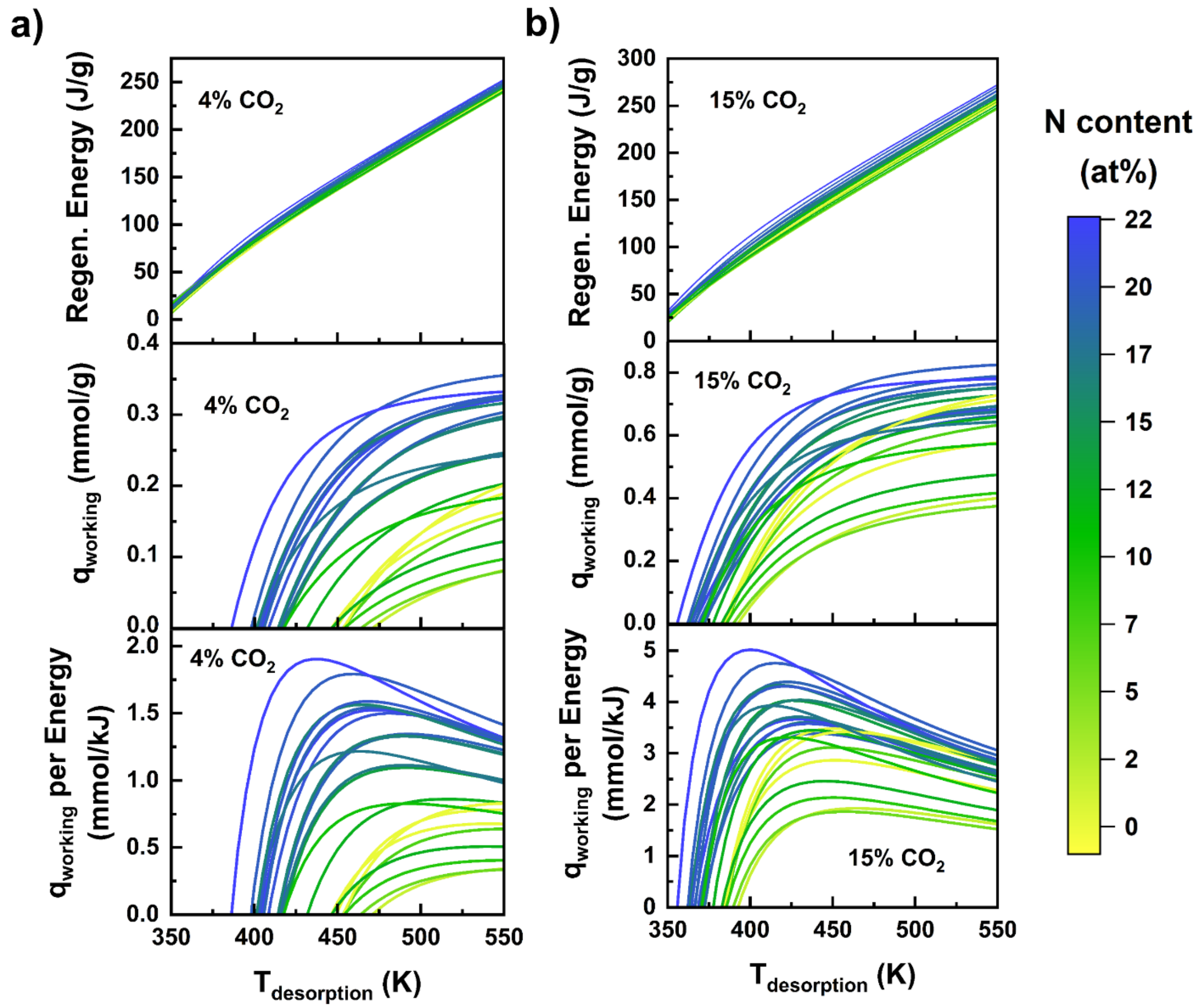

Figure S15. Predicted regeneration energy (top), working capacity (middle), and figure of merit – working capacity per energy (bottom) for a simplified TSA process considering a feed with a) 4% and b) 15% CO_2.

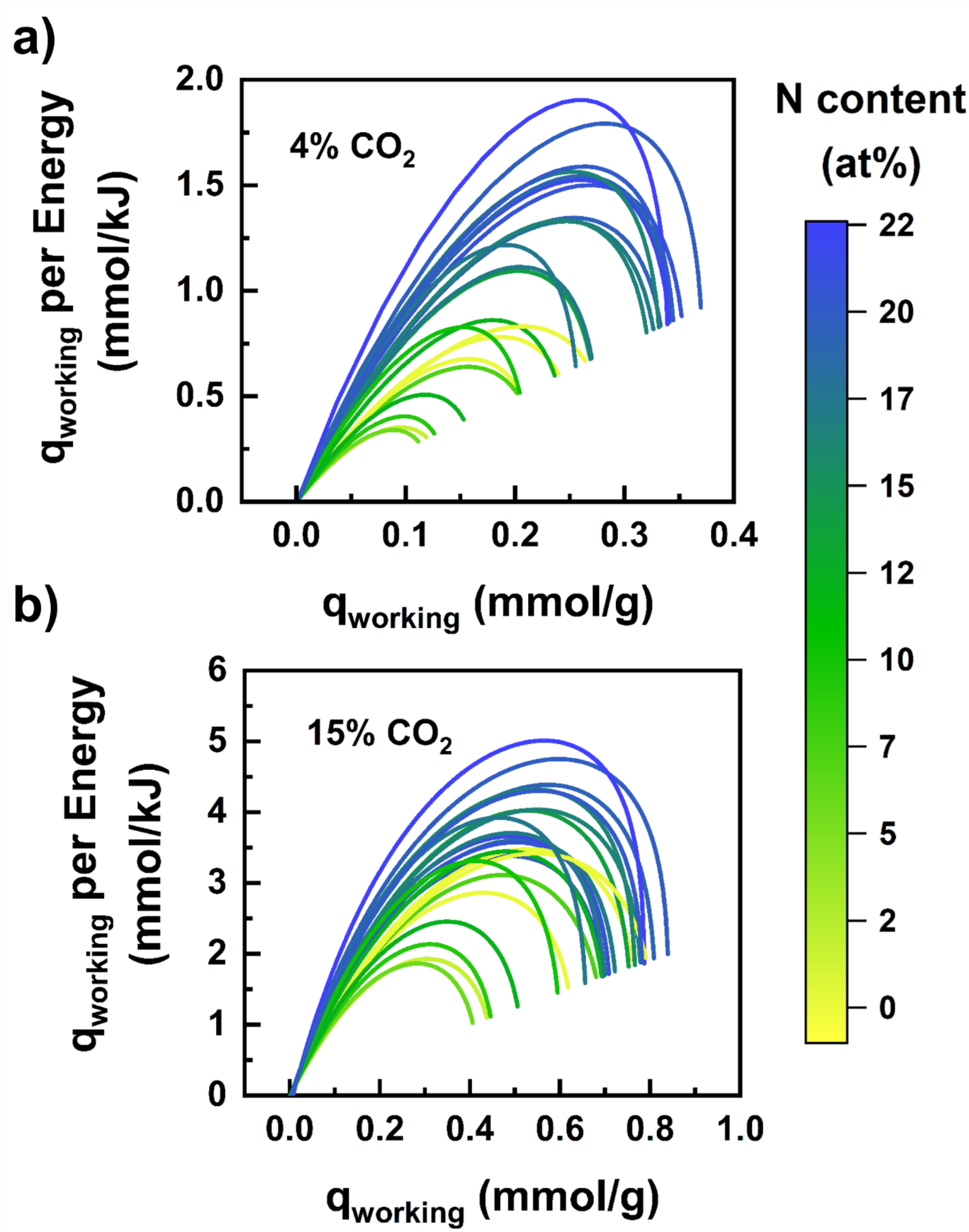

Figure S16. Curves representing the achievable combinations of working capacity and working capacity per energy, showing how for each of the CO_2 feed stream under consideration (4%, a; 15%, b), an optimal regeneration temperature exists.

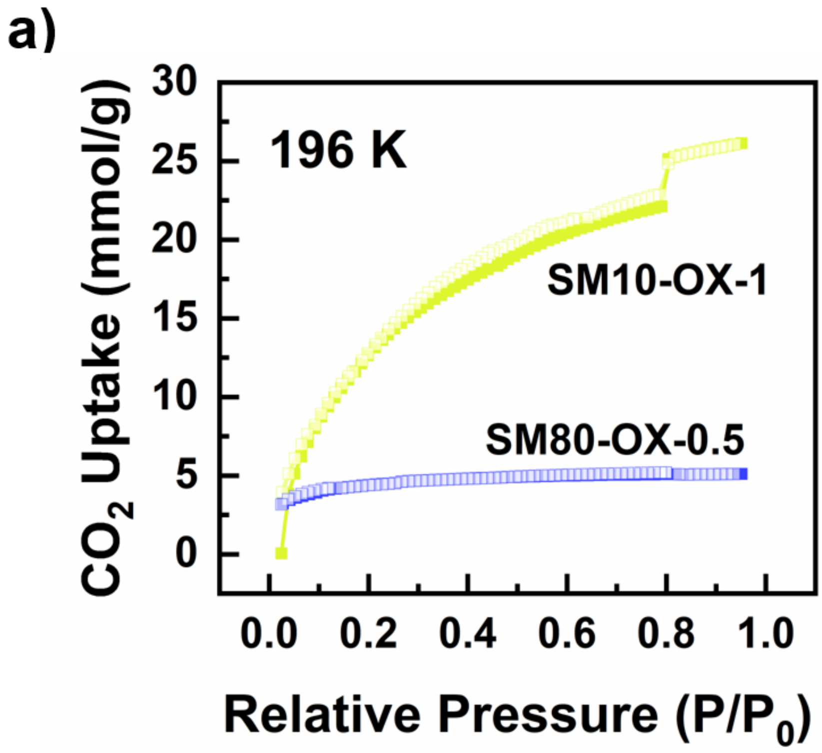

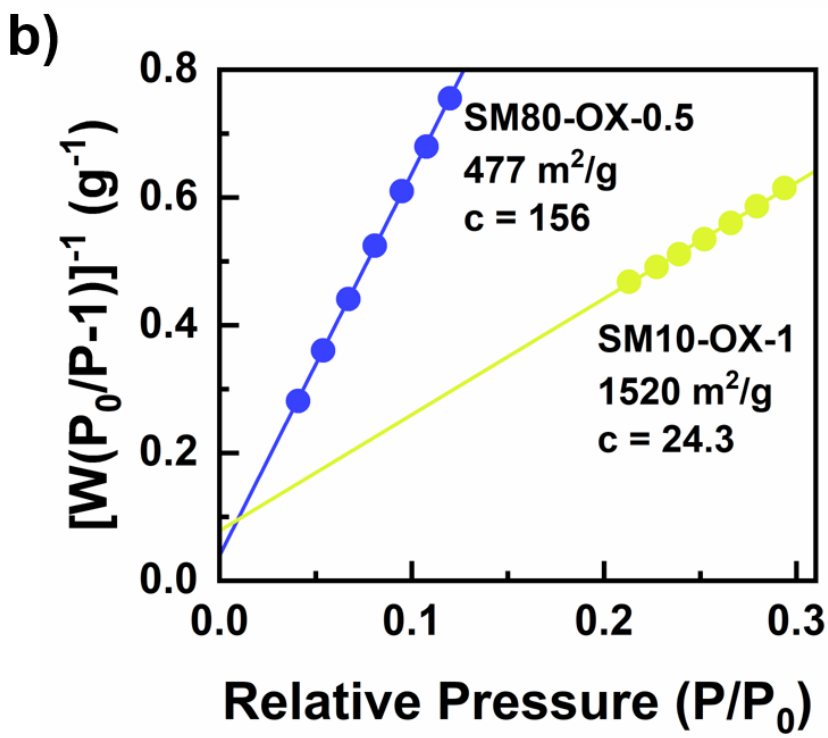

Figure S17. a) Isotherms and b) BET analysis of an N-rich sample (SM80-OX-0.5, blue) and an N-poor sample (SM10-OX-1, yellow) employing CO_2 (instead of N_2) as an adsorbate/probe molecule at 195 K.